NANO LETTERS

Letter

pubs.acs.org/NanoLett

Universal, In Situ Transformation of Bulky Compounds into Nanoscale Catalysts by High-Temperature Pulse

Shaomao Xu, Yanan Chen, Yiju Li, Aijiang Lu, Yonggang Yao, Jiaqi Dai, Yanbin Wang, Boyang Liu, Steven D. Lacey, Glenn R. Pastel, Yudi Kuang, Valencia A. Danner, Feng Jiang, Kun Kelvin Fu, and Liangbing Hu*

Department of Materials Science and Engineering, University of Maryland College Park, College Park, Maryland 20742, United States

Supporting Information

ABSTRACT: The synthesis of nanoscale metal compound catalysts has attracted much research attention in the past decade. The challenges of preparation of the metal compound include the complexity of the synthesis process and difficulty of precise control of the reaction conditions. Herein, we report an in situ synthesis of nanoparticles via a high-temperature pulse method where the bulk material acts as the precursor. During the process of rapid heating and cooling, swift melting, anchoring, and recrystallization occur, resulting in the generation of high-purity nanoparticles. In our work, the cobalt boride (Co_2B) nanoparticles with a diameter of 10−20 nm uniformly anchored on the reduced graphene oxide (rGO) nanosheets were successfully prepared using the high temperature pulse method. The as-prepared Co_2B/rGO composite displayed remarkable electrocatalytic performance for the hydrogen evolution reaction (HER) and oxygen evolution reaction (OER). We also prepared molybdenum disulfide (MoS_2) and cobalt oxide (Co_3O_4) nanoparticles, thereby demonstrating that the high-temperature pulse is a universal method to synthesize ultrafine metal compound nanoparticles.

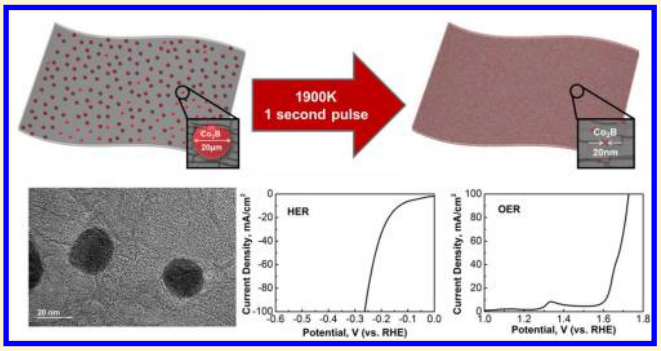

KEYWORDS: *High temperature, rapid synthesis, in situ formation, water splitting, nanoscale catalyst*

Due to increasing global energy consumption, alternative energy sources are a high priority to replace non-renewable fossil fuels.[1] Hydrogen has been considered the most promising replacement for fossil fuels due to its ultrahigh energy density and negligible amount of greenhouse gas emission.[2−6] The hydrogen production through water splitting by electrocatalysis is regarded as the most promising method.[7−9] The conventional electrocatalysts used in water splitting are noble metal-based materials, including platinum (Pt), ruthenium (Ru), palladium (Pd), and iridium (Ir).[10−12] However, the high cost of these catalysts inhibits the large-scale applications. Researchers have made numerous efforts to explore the replacement of noble metals with low-cost catalysts as well with favorable electrochemical performance. Transitional metal chalcogenides,[13−19] oxides,[20−22] and other transitional metal compounds (carbides, nitrides, borides, phosphides, etc.) with relatively low cost have be widely investigated recently.[23,24] However, conventional preparation processes are usually involved with high pressure and temperature, such as the hydrothermal method and programmed heating in a tubular furnace, which are complicated and sensitive. A fast and effective method to synthesize metal compound nanoparticles is appealing for the future development and commercialization of high-performance electrocatalysts.

In this work, for the first time, we report an easy and rapid synthesis method to produce nanosized catalysts directly from a bulk precursor. To demonstrate this method, cobalt boride (Co_2B) catalyst nanoparticles were produced and studied.[24−26] The bulk Co_2B precursor (micron size) can be converted to ultrafine nanoparticles with a diameter of 10−20 nm by the high temperature pulse.[27] After the high temperature treatment, the nanosized Co_2B catalysts are evenly distributed across the rGO sheets. The Co_2B nanoparticles/rGO composite film shows an excellent electrochemical performance of water splitting and superior cycling stability. We also successfully prepared the molybdenum disulfide (MoS_2) and cobalt oxide (Co_3O_4) nanoparticles using the high-temperature pulse. The high-temperature pulse method offers a new synthesis route toward nanoscale metal compound catalysts.

Results and Discussion. Our high-temperature pulse method used to synthesize nanoscale Co_2B is illustrated in Figure 1. The Co_2B bulk precursor was prepared through the reaction of sodium borohydride ($NaBH_4$) with cobalt acetate ($CoAc_2$) solution, which is reported in other literature.[28,29] The formed Co_2B microparticles were mixed with graphene oxide solution with continuous stirring. The mixture was then casted onto a flat glass slide and prereduced to form the Co_2B bulk/rGO composite film. The Co_2B bulk is uniformly dispersed into

Received: July 15, 2017
Published: August 3, 2017

DOI: 10.1021/acs.nanolett.7b03019
Nano Lett. 2017, 17, 5817−5822

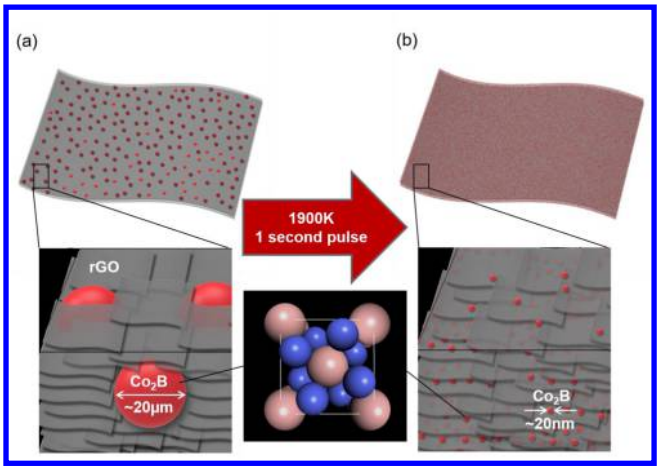

Figure 1. Schematic of Co_2B nanoparticle synthesis by a novel high-temperature pulse treatment. (a) After the chemical reaction between $NaBH_4$ and $CoAc_2$, Co_2B microparticles are wrapped within the rGO film. (b) After the high-temperature pulse procedure, the Co_2B microparticles transform into ultrafine nanoparticles with a diameter of ~20 nm that uniformly decorate on the rGO sheets. The inset shows the crystal structure of Co_2B, which is maintained after the high-temperature pulse.

the rGO film (Figure 1a and S1). After treatment of a high-temperature pulse using the Joule heating under argon atmosphere (temperature: 1900 K; time: 1 s), the Co_2B microparticles are successfully converted into ultrafine nanoparticles with a diameter of ~20 nm (Figure 1b). No obvious change in the Co_2B weight and no remnants of the Co_2B micropowders were observed after the heat pulse treatment. Note that the structure of nanoparticles/rGO composite film has been successfully employed in a range of applications including catalysis.[30−32]

The light emission spectra associated with the Joule heating process is shown in Figure 2a. The temperature was determined by the radiation intensity emitted by the sample in relation to blackbody theory. The highest heating temperature reached 1933 K based on the spectral radiation fitting. The temperature ramp time for the high-temperature pulse treatment is as short as a few milliseconds (Figure 2b). Note that the cooling time is within a similar time frame. The swift heating and cooling steps lead to the rapid melting and recrystallization of Co_2B, respectively. Therefore, this unique synthesis method enables the formation of nanosized Co_2B even though a bulk precursor was employed. Additionally, due to the short current pulse flowing through the rGO film, the rGO becomes exfoliated. Thus, some wrinkled features on the rGO sheets form due to the heating pulse (Figure 2b insets).

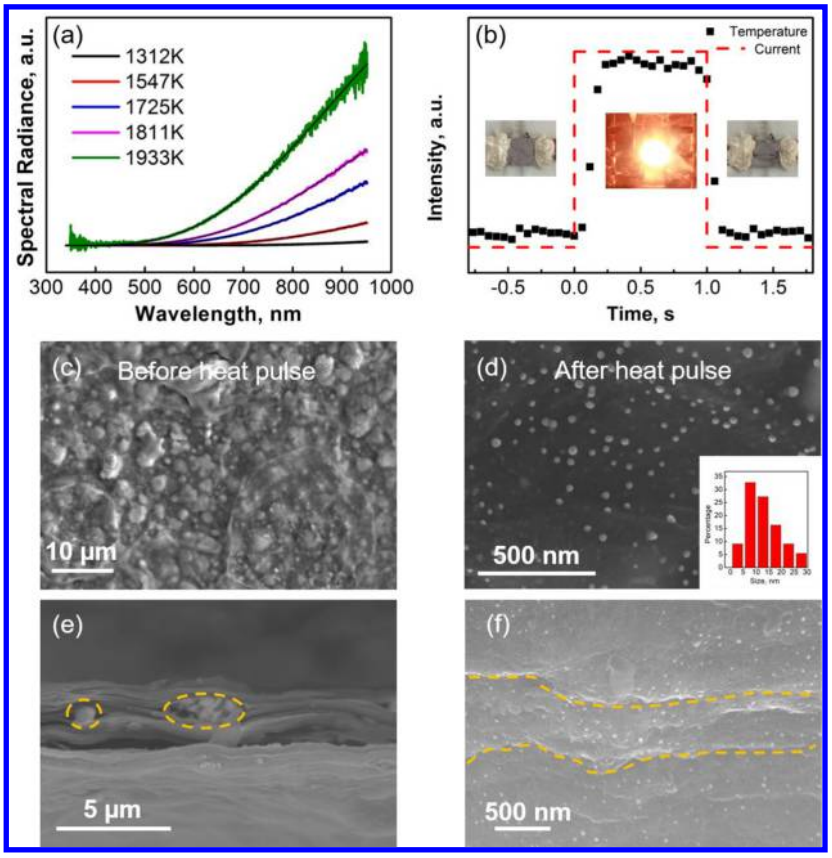

Figure 2. Characterization of the heating procedure and the resulting material. (a) Light emission spectra during the temperature ramp stage. A final temperature of 1933 K is reached during the heating. (b) Light intensity and current applied throughout the short high-temperature pulse. Insets are digital photos of the rGO with Co_2B before, during and after the heating pulse, respectively. (c) SEM image of the rGO film surface before the high-temperature pulse. The Co_2B are microsized particles. (d) SEM image of the rGO film surface after the high-temperature pulse. The Co_2B nanoparticles (10−20 nm) are evenly distributed on the rGO sheets. Insets show the size distribution of the nanoparticles. (e) Cross-sectional SEM image of the rGO film before the high-temperature pulse, where large Co_2B particles are embedded between the rGO layers. (f) SEM image of several rGO film layers after the high-temperature pulse. The Co_2B nanoparticles are densely packed throughout the rGO layers.

DOI: 10.1021/acs.nanolett.7b03019
Nano Lett. 2017, 17, 5817−5822

The morphology of the Co_2B-embedded rGO film before and after the high temperature pulse was studied via scanning electron microscopy (SEM) (Figure 2c–f). Before the heating pulse, Co_2B particles (tens of micrometers in diameter) covered the surface of the rGO film (Figure 2c) as well as occupied spaces between the graphene-like layers (Figure 2e). After a rapid one-second heating pulse, the microsized Co_2B particles transformed into uniformly distributed nanoparticles across the entire rGO film surface (Figure 2d). Note that the morphology of the rGO film after heat pulse treatment is different from the pristine rGO film (Figure S2). Numerous Co_2B nanoparticles decorating the rGO film can be observed, which are absent on the pristine rGO films. A uniform nanoparticle distribution is crucial to offer abundant electrochemical active sites during the water splitting process. The detailed calculations of the active surface of the Co_2B/rGO film are shown in the Supporting Information (Figure S3). Beyond the surface layer, the inner rGO film layers are also decorated with Co_2B nanoparticles. Figure 2f reveals the morphology of these inner layers, which coincides with the catalyst-decorated surface layer. The interlayer spacing of the rGO increased after the heating pulse due to the current flow. The structure enables the accessibility of electrolyte to the inner of the rGO film, which can improve the catalytic activity of the as-prepared material. The narrow size distribution of the Co_2B particles (10–20 nm) further enhances the contact between the water molecules and the catalytically active nanoparticles (Figure S4). These unique features validate Co_2B nanoparticle-decorated rGO as a suitable catalyst material for the electrolysis of water splitting.

The composition of the Co_2B nanoparticles was confirmed by energy-dispersive X-ray (EDX) and X-ray diffraction (XRD) analyses. The EDX spectrum (Figure S5a) shows distinct peaks corresponding to the energy of boron, carbon, and cobalt. The atomic ratio between cobalt and boron is nearly 2:1, which is consistent with the stoichiometric value of the reported compound: Co_2B. Figure S5b shows an XRD peak at 45.8° which corresponds to the (211) of Co_2B. This is the characteristic peak for Co_2B and confirms its crystallographic structure.[24−26] The peaks at 27° and 29.4° are consistent with previously reported XRD peaks for reduced graphene oxide.[33,34] Thus, it can be concluded that the crystal structure of the Co_2B nanoparticles remains unchanged after a high-temperature pulse.

TEM and elemental maps confirm the structure and composition of the synthesized Co_2B catalyst. Figure 3a–b shows that 10–20 nm particles are uniformly distributed and embedded within the rGO film, which is consistent with the SEM images. Note that the Co_2B nanoparticles are spherical with a diameter of 20 nm. In the high-resolution TEM image, a lattice spacing of 2.1 Å is obtained (Figure 3c). This value is consistent with the structure of Co_2B as well as previous reports.[24] The elemental map of the Co_2B nanoparticle also matches well with the qualitative distribution of cobalt (Figure 3d–e). Therefore, the facile and rapid high-temperature pulse method is capable of synthesizing nanosized metal compounds directly from bulk precursors.

The unique morphology introduced by the high-temperature pulse method leads to significant improvements in catalytic activity. The electrochemical tests for HER and OER as well as the overall water splitting performance of the as-prepared catalyst material are shown in Figure 4. For the HER activity test, the Co_2B-decorated electrode acts as the cathode. Figure 4a shows an onset HER overpotential as low as 33 mV.

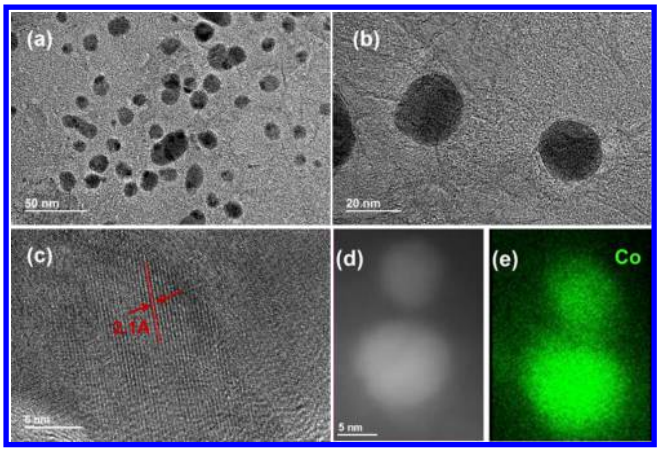

Figure 3. TEM images of Co_2B nanoparticles after the high temperature pulse. (a–b) TEM images showing that the particles are evenly distributed on the rGO film with a uniform size around 20 nm. (c) High-resolution TEM image indicating the lattice spacing of the Co_2B particle is 2.1 Å. (d) Dark-field image of the nanoscale Co_2B. (e) EDX map of the elemental cobalt where the distribution matches well with the nanoparticles synthesized with the high-temperature pulse treatment.

Additionally, at an overpotential of 260 mV, the current density reaches 100 mA/cm^2, which places the synthesized Co_2B nanoparticles among the most effective HER catalysts.[35−39] The HER activity of the Co_2B/rGO composite film increases remarkably compared to bare rGO film (Figure S6). Note that the current density of the Co_2B nanoparticles is five times higher compared to the same material synthesized via different routes,[24] indicating the remarkable advantage of the high-temperature pulse synthesis. The Tafel slope can be used to analyze the reaction mechanism and rate-limiting step.[35,36] According to the Bulter–Volmer kinetics, the Tafel slope of 118, 39, or 29.5 mV/dec indicates that the Volmer, Heyrovsky, or Tafel reaction is rate-determining, respectively. In our work, for the HER, the Tafel slope is 96 mV/dec, which suggests that the HER occurs through the Volmer–Heyrovsky mechanism.

The long-term stability of the catalyst material is another important parameter. Linear sweep voltammetry (Figure S7) as well as constant potential tests under harsh conditions (Figure 4c) are employed to study the stability of the synthesized Co_2B nanocatalyst. After 1000 cycles, there is a slight overpotential shift of 25 mV, which corresponds to an overpotential of 380 mV at 100 mA/cm^2 and illustrates the excellent stability of the Co_2B nanoparticles under prolonged operation. When a constant overpotential of 170 mV is applied to the Co_2B electrode, the current density remains at a constant value of 18 mA/cm^2 with no decay after a 10 h period. The results indicate that the Co_2B nanoparticles act as a stable HER catalyst and can sustain long-term application under a high work load. The same materials prior to the high-temperature pulse treatment do not exhibit catalytic activity. Thus, the reported synthesis method enables the formation of nanocatalysts with an excellent electrolytic activity.

Similar tests were performed when the Co_2B nanoparticle operated as the anode (OER reaction) during the electrolysis of water. Figure 4d displays an onset potential of 1.59 V (vs RHE) for the oxygen evolution reaction, which corresponds to an onset overpotential as low as 360 mV. The calculated Tafel slope is extremely low (85.4 mV/dec), which corresponds to excellent OER activity (Figure 4e). Note that the OER activity

DOI: 10.1021/acs.nanolett.7b03019
Nano Lett. 2017, 17, 5817–5822

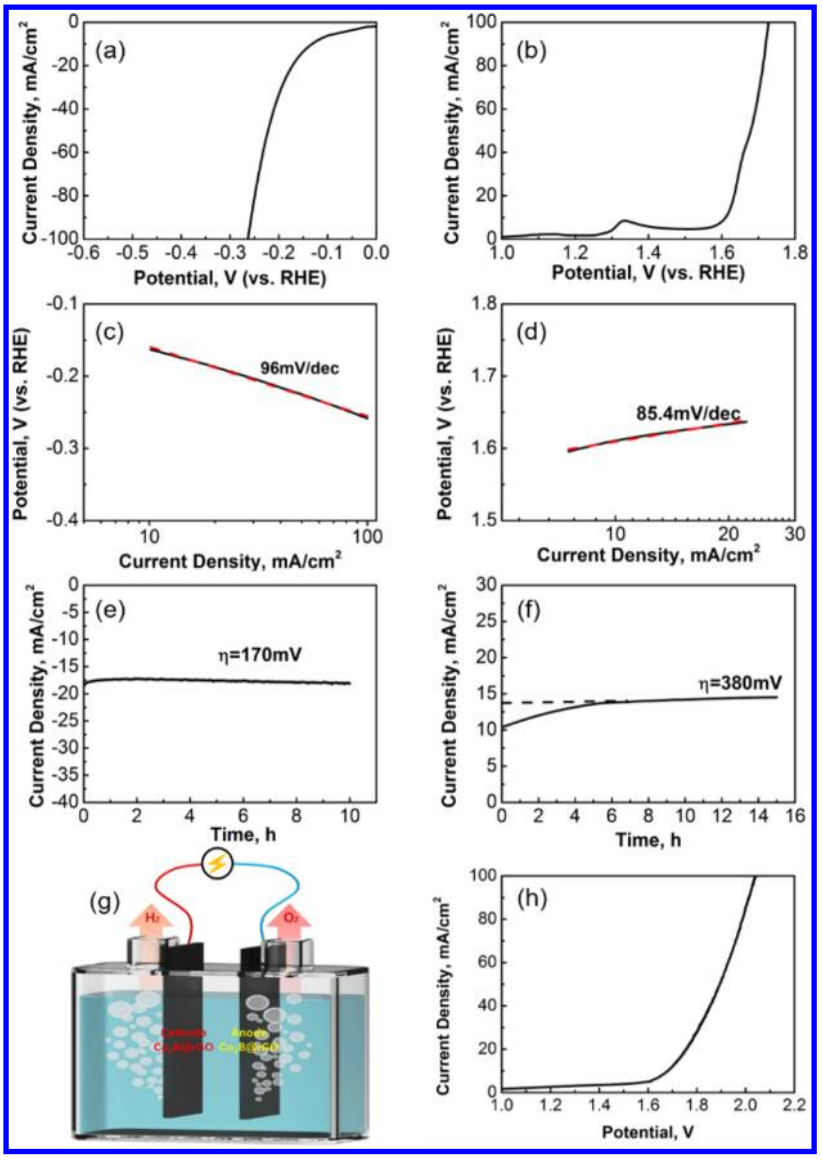

Figure 4. Catalytic activity of the synthesized Co_2B nanoparticles. (a) Polarization curve of the HER reaction in a 0.5 M H_2SO_4 solution. (b) Polarization curve of OER in a 1 M KOH solution. (c) Tafel plot of the HER test with a Tafel slope of 96 mV/dec. (d) Tafel plot of the OER test with a Tafel slope of 85.4 mV/dec. (e) Constant voltage test for HER. No current density decay was observed after 10 h, indicating remarkable HER stability. (f) Constant voltage test for OER. After a short activation period, the current density reaches a stable value of 13.5 mA/cm^2. No current density decay was observed after 15 h, indicating excellent OER stability. The dashed line indicates the activation period. (g) Schematic showing the water splitting experimental setup. The Co_2B nanoparticles embedded in rGO are used as both the anode and the cathode for electrolysis. (h) Linear sweep voltammetry curve of the overall water splitting process.

of the Co_2B nanocatalyst coincides with a previously reported value for Co_2B synthesized via a more conventional route.[24] When an overpotential of 380 mV is applied to the electrode, the current density reaches a constant value of 13.5 mA/cm^2 and remains unchanged for 15 h after a short activation period (Figure 4f). The remarkable activity and sustainability of the synthesized Co_2B nanoparticles under long-term operation is comparable to some of the best OER catalysts reported to date.[40−45]

To demonstrate the use of Co_2B as both the anode and the cathode in the water splitting process, a single electrolyzer was employed. A schematic of the experimental setup is shown in Figure 4g. Figure 4h shows the polarization curve of the overall water splitting process. The potentials at 10, 50, and 100 mA/cm^2 are 1.67, 1.87, and 2.03 V, respectively. The low potentials at high current densities indicate the excellent bifunctionality of the Co_2B nanocatalyst. Therefore, the synthesized Co_2B nanoparticles/rGO film electrode via the high-temperature pulse method is a highly active bifunctional HER/OER catalyst with remarkable stability.

To understand the nanoparticle formation mechanism of the high-temperature pulse synthesis method, a theoretical model was developed. Molecular dynamics (MD) simulations were adopted to compare with the aforementioned experimental results. The Forcite module, within Material Studio, was employed with a universal force field and medium quality to ensure balance between computational cost and modeling precision. First, an amorphous Co_2B bulk was constructed using a supercell of 384 atoms. Since the pulse heating time is miniscule, the abrupt increase in temperature is simulated through MD calculations. When the Co_2B is rapidly heated above 1900 K, the material melts and is trapped by defects

DOI: 10.1021/acs.nanolett.7b03019
Nano Lett. 2017, 17, 5817−5822

(oxygen-containing functional groups) on rGO sheets. When the high temperature pulse stops (cooling process), the Co_2B nanoparticles are in situ formed. Figure S8 shows the melting and reconstruction of the Co_2B crystalline structure based on the radial distribution function (RDF). The vacuum seam formed during the cooling duration results in the separation between Co_2B nanoclusters.

The effect of heating time is essential to synthesizing catalytically active materials with excellent performance. Specifically, faster heating is required to achieve nanoscale catalysts with more uniform particle distributions. When a short pulse (1 s) is applied to the Co_2B material, the diameter of the obtained Co_2B nanoparticles is about 20 nm. However, when the heating time is extended to 1 min, the clusters grow to a few hundred nanometers in diameter. We hypothesize that, during the high-temperature pulse, the Co_2B melts and is trapped by the defects on the rGO sheets. When the pulse is off (cooling process), the Co_2B nanoparticles are in situ formed. To obtain the lowest surface energy, sphere-like nanoparticles with good crystallinity are formed. When the heating time increases, the defects on the rGO sheets will decrease. During the cooling period, there are fewer defects to trap Co_2B nanoparticles. Therefore, the Co_2B nanoparticles will aggregate, and the size will increase. Figure 5a–b illustrates the heating processes and

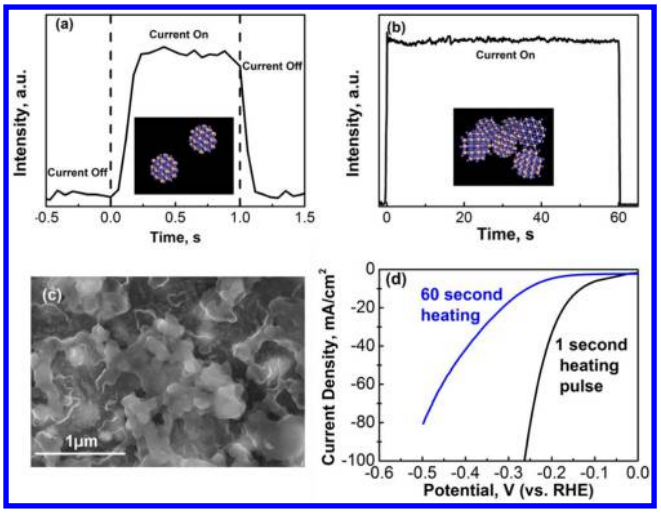

Figure 5. Effect of heating time on the synthesized material. (a) The light intensity during the one second high-temperature pulse heating. Inset shows that the Co_2B forms separate nanoparticles based on the simulation results. (b) The light intensity during the 1 min high-temperature treatment. Inset shows that the Co_2B nanoparticles agglomerate and form larger clusters. (c) SEM image of the Co_2B synthesized after a 1 min heat treatment. The nanoparticles agglomerate under prolonged heating time, which confirms the importance of the rapid one second synthesis. The large clusters observed are consistent with the simulation in panel b. (d) Comparison of the HER activity between Co_2B synthesized with a one second high-temperature pulse and by prolonged 1 min heating. The prolonged heating results in loss of catalytic activity, confirming the crucial role of a short heating pulse.

the respective morphologies of the Co_2B during the high-temperature pulse treatment. With the increase in heating time, the size of the Co_2B nanoparticles increases, and the Co_2B nanoparticles gradually aggregate (Figure S9). Our simulation results match well with the SEM image shown in Figure 5c since the profile of the connected nanoclusters denotes a coral-like morphology. The heating time also has an extensive effect on the particle's catalytic activity. The HER activities of Co_2B synthesized with a one second high-temperature pulse as well as prolonged 1 min heating is compared in Figure 5d. Specifically, the sample under prolonged heating has a much lower catalytic activity due to the agglomeration of Co_2B nanoparticles. These results indicate that controlling the heating time of the high-temperature treatment is crucial to achieve a suitable morphology and catalytic activity of the resulting material.

Herein, we point out that the synthesis method reported here is not unique to Co_2B nanoparticles. To demonstrate the universality of the proposed method, molybdenum disulfide (MoS_2, Figure 6a–b) and cobalt oxide (Co_3O_4, Figure 6c–d)

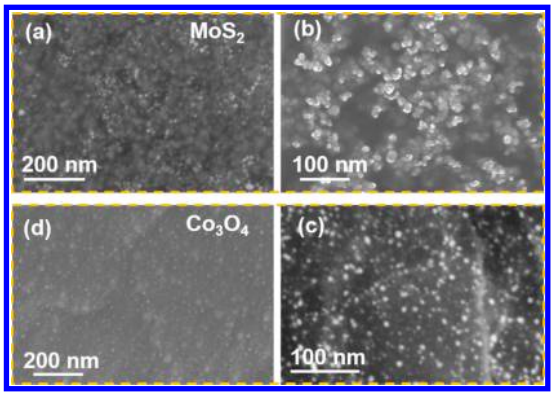

Figure 6. Universality demonstration of the high-temperature pulse method. SEM images of (a–b) MoS_2 and (c–d) Co_3O_4 nanoparticles synthesized by rapid high-temperature treatment.

nanoparticles were also successfully synthesized using the high temperature pulse. XRD measurements (Figure S10) confirm the crystal structures of the synthesized materials. The tested XRD patterns match the standard curves of MoS_2 and Co_3O_4, respectively, and no other impurity peaks are observed.[13,16,46] Compared to the previously reported high-temperature methods for preparing nanoparticles, our high-temperature pulse with rapid heating and cooling contributes to the fast formation of ultrasmall nanoparticles. Additionally, Joule heating is much more efficient than conventional heating methods (thermal-radiation heating: energy- and time-consuming).[47,48] Therefore, a range of compound nanoparticles can be successfully synthesized directly from bulk precursors via the high-temperature pulse method, which can be applied in catalytic applications and beyond.

Conclusion. In summary, for the first time, we reported a simple and universal in situ preparation method to directly convert the precursors of compound bulk to nanoparticles using the high-temperature pulse. Compared with the conventional high-temperature preparation methods, the high-temperature pulse is facile, fast, and efficient. During the fast process of preparation, swift melting, anchoring, and recrystallization occur successively, which can generate numerous high-purity nanoparticles. The ultrafine cobalt boride (Co_2B) nanoparticles uniformly dispersed on the rGO sheets were successfully synthesized using the high-temperature pulse method (temperature: 1900 K; time: 1 s). The obtained Co_2B/rGO composite film showed superior electrocatalytic performance for water splitting. In our work, the MoS_2 and Co_3O_4 nanoparticles were also successfully prepared using the heat pulse, which demonstrates that the universality of the high-temperature

DOI: 10.1021/acs.nanolett.7b03019
Nano Lett. 2017, 17, 5817–5822

pulse method. The preparation method of a high-temperature pulse is a promising approach to rapidly and efficiently prepare compound nanoparticles.

■ ASSOCIATED CONTENT

Supporting Information

The Supporting Information is available free of charge on the ACS Publications website at DOI: 10.1021/acs.nanolett.7b03019.

Experimental section (PDF)

■ AUTHOR INFORMATION

Corresponding Author

*E-mail: binghu@umd.edu.

ORCID

Liangbing Hu: 0000-0002-9456-9315

Author Contributions

S.X., Y.C., and Y.L. contributed equally to this work.

Notes

The authors declare no competing financial interest.

■ ACKNOWLEDGMENTS

This project is supported by the NSF Project no. 1635221. We acknowledge the support of the Maryland NanoCenter and its AIMLab.

■ REFERENCES

(1) Weisz, P. B. *Phys. Today* **2004**, *57*, 47−52.
(2) Bockris, J. O. M. *Int. J. Hydrogen Energy* **2002**, *27*, 731−740.
(3) Dresselhaus, M. S.; Thomas, I. L. *Nature* **2001**, *414*, 332−337.
(4) Turner, J. A. *Science* **2004**, *305*, 972−974.
(5) Lewis, N. S.; Nocera, D. G. *Proc. Natl. Acad. Sci. U. S. A.* **2006**, *103*, 15729−15735.
(6) Walter, M. G.; Warren, E. L.; McKone, J. R.; Boettcher, S. W.; Mi, Q.; Santori, E. A.; Lewis, N. S. *Chem. Rev.* **2010**, *110*, 6446−6473.
(7) Faber, M. S.; Jin, S. *Energy Environ. Sci.* **2014**, *7*, 3519−3542.
(8) Thoi, V. S.; Sun, Y.; Long, J. R.; Chang, C. J. *Chem. Soc. Rev.* **2013**, *42*, 2388−2400.
(9) Yang, X.; Liu, R.; He, Y.; Thorne, J.; Zheng, Z.; Wang, D. *Nano Res.* **2015**, *8*, 56−81.
(10) Esposito, D. V.; Hunt, S. T.; Kimmel, Y. C.; Chen, J. G. *J. Am. Chem. Soc.* **2012**, *134*, 3025−3033.
(11) Kelly, T. G.; Lee, K. X.; Chen, J. G. *J. Power Sources* **2014**, *271*, 76−81.
(12) Greeley, J.; Jaramillo, T. F.; Bonde, J.; Chorkendorff, I. B.; Norskov, J. K. *Nat. Mater.* **2006**, *5*, 909−913.
(13) Zhang, X.; Lai, Z.; Tan, C.; Zhang, H. *Angew. Chem., Int. Ed.* **2016**, *55*, 8816−8838.
(14) Kong, D.; Cha, J. J.; Wang, H.; Lee, H. R.; Cui, Y. *Energy Environ. Sci.* **2013**, *6*, 3553−3558.
(15) Kong, D.; Wang, H.; Lu, Z.; Cui, Y. *J. Am. Chem. Soc.* **2014**, *136*, 4897−4900.
(16) Kong, D.; Wang, H.; Cha, J. J.; Pasta, M.; Koski, K. J.; Yao, J.; Cui, Y. *Nano Lett.* **2013**, *13* (3), 1341−1347.
(17) Wang, H.; Lu, Z.; Kong, D.; Sun, J.; Hymel, T. M.; Cui, Y. *ACS Nano* **2014**, *8*, 4940−4947.
(18) Miao, J.; Xiao, F.-X.; Yang, H. B.; Khoo, S. Y.; Chen, J.; Fan, Z.; Hsu, Y.-Y.; Chen, H. M.; Zhang, H.; Liu, B. *Sci. Adv.* **2015**, *1* (7), e1500259.
(19) Zhang, H.; Ding, Q.; He, D.; Liu, H.; Liu, W.; Li, Z.; Yang, B.; Zhang, X.; Lei, L.; Jin, S. *Energy Environ. Sci.* **2016**, *9*, 3113−3119.
(20) Lin, Y.; Yuan, G.; Sheehan, S.; Zhou, S.; Wang, D. *Energy Environ. Sci.* **2011**, *4*, 4862−4869.
(21) Wang, H.; Lee, H.-W.; Deng, Y.; Lu, Z.; Hsu, P.-C.; Liu, Y.; Lin, D.; Cui, Y. *Nat. Commun.* **2015**, *6*, 7261.
(22) Li, W.; He, D.; Sheehan, S. W.; He, Y.; Thorne, J. E.; Yao, X.; Brudvig, G. W.; Wang, D. *Energy Environ. Sci.* **2016**, *9*, 1794−1802.
(23) Cabán-Acevedo, M.; Stone, M. L.; Schmidt, J. R.; Thomas, J. G.; Ding, Q.; Chang, H.-C.; Tsai, M.-L.; He, J.-H.; Jin, S. *Nat. Mater.* **2015**, *14*, 1245−1251.
(24) Masa, J.; Weide, P.; Peeters, D.; Sinev, I.; Xia, W.; Sun, Z.; Somsen, C.; Muhler, M.; Schuhmann, W. *Adv. Energy Mater.* **2016**, *6*, 1502313.
(25) Krishnan, P.; Advani, S. G.; Prasad, A. K. *Int. J. Hydrogen Energy* **2008**, *33*, 7095−7102.
(26) Delmas, J.; Laversenne, L.; Rougeaux, I.; Capron, P.; Garron, A.; Bennici, S.; Świerczyński, D.; Auroux, A. *Int. J. Hydrogen Energy* **2011**, *36*, 2145−2153.
(27) Bao, W.; Pickel, A. D.; Zhang, Q.; Chen, Y.; Yao, Y.; Wan, J.; Fu, K.; Wang, Y.; Dai, J.; Zhu, H.; Drew, D.; Fuhrer, M.; Dames, C.; Hu, L. *Adv. Mater.* **2016**, *28*, 4684−4691.
(28) Carenco, S.; Portehault, D.; Boissiere, C.; Mezailles, N.; Sanchez, C. *Chem. Rev.* **2013**, *113*, 7981−8061.
(29) Glavee, G. N.; Klabunde, K. J.; Sorensen, C. M.; Hadjipanayis, G. C. *Langmuir* **1993**, *9*, 162−169.
(30) Ping, J.; Wang, Y.; Lu, Q.; Chen, B.; Chen, J.; Huang, Y.; Ma, Q.; Tan, C.; Yang, J.; Cao, X.; Wang, Z.; Wu, J.; Ying, Y.; Zhang, H. *Adv. Mater.* **2016**, *28*, 7640−7645.
(31) El-Kady, M. F.; Shao, Y.; Kaner, R. B. *Nat. Rev. Mats.* **2016**, *1*, 16033.
(32) Wassei, J. K.; Kaner, R. B. *Acc. Chem. Res.* **2013**, *46*, 2244−2253.
(33) Cui, P.; Lee, J.; Hwang, E.; Lee, H. *Chem. Commun.* **2011**, *47*, 12370−12372.
(34) Drewniak, S.; Muzyka, R.; Stolarczyk, A.; Pustelny, T.; Kotyczka-Moranska, M.; Setkiewicz, M. *Sensors* **2016**, *16*, 103.
(35) Zeng, M.; Li, Y. *J. Mater. Chem. A* **2015**, *3*, 14942−14962.
(36) Zou, X.; Zhang, Y. *Chem. Soc. Rev.* **2015**, *44*, 5148−5180.
(37) Fei, H.; Dong, J.; Arellano-Jimenez, M. J.; Ye, G.; Kim, N. D.; Samuel, E. L. G.; Peng, Z.; Zhu, Z.; Qin, F.; Bao, J.; Yacaman, M. J.; Ajayan, P. M.; Chen, D.; Tour, J. M. *Nat. Commun.* **2015**, *6*, 8668.
(38) Zhang, J.; Zhao, Z.; Xia, Z.; Dai, L. *Nat. Nanotechnol.* **2015**, *10*, 444−452.
(39) Zhang, J.; Qu, L.; Shi, G.; Liu, J.; Chen, J.; Dai, L. *Angew. Chem.* **2016**, *128*, 2270−2274.
(40) Xia, B. Y.; Yan, Y.; Li, N.; Wu, H. B.; Lou, X. W.; Wang, X. *Nat. Energy* **2016**, *1*, 15006.
(41) Xu, L.; Jiang, Q.; Xiao, Z.; Li, X.; Huo, J.; Wang, S.; Dai, L. *Angew. Chem.* **2016**, *128*, 5363−5367.
(42) Dou, S.; Tao, L.; Huo, J.; Wang, S.; Dai, L. *Energy Environ. Sci.* **2016**, *9*, 1320−1326.
(43) Burke, M. S.; Enman, L. J.; Batchellor, A. S.; Zou, S.; Boettcher, S. W. *Chem. Mater.* **2015**, *27*, 7549−7558.
(44) Fan, Z.; Luo, Z.; Chen, Y.; Wang, J.; Li, B.; Zong, Y.; Zhang, H. *Small* **2016**, *12* (29), 3908−3913.
(45) Feng, J.; Ye, S.; Xu, H.; Tong, Y.; Li, G. *Adv. Mater.* **2016**, *28*, 4698−4703.
(46) Liang, Y.; Li, Y.; Wang, H.; Zhou, J.; Wang, J.; Regier, T.; Dai, H. *Nat. Mater.* **2011**, *10*, 780−786.
(47) Unni, M.; Uhl, A. M.; Savliwala, S.; Savitzky, B. H.; Dhavalikar, R.; Garraud, N.; Arnold, D. P.; Kourkoutis, L. F.; Andrew, J. S.; Rinaldi, C. *ACS Nano* **2017**, *11*, 2284−2303.
(48) Sun, S.; Zeng, H. *J. Am. Chem. Soc.* **2002**, *124* (28), 8204−8205.

DOI: 10.1021/acs.nanolett.7b03019
Nano Lett. 2017, 17, 5817−5822